IJCRT.ORG ISSN : 2320-2882

INTERNATIONAL JOURNAL OF CREATIVE RESEARCH THOUGHTS (IJCRT)

An International Open Access, Peer-reviewed, Refereed Journal

Novel Palladium, Cerium-Schiff Base Complex: A Dual-Action Agent Against Breast Cancer (MCF-7), Bacterial Pathogens And Molecular Docking With ADME Studies

[1]Periyannan Muniyappan, [2]Santhakumar Munusamy and [3]Rajavel Rangappan*

[1,2] Ph. D Research Scholar, [3]Professor

[1,3] Department of Chemistry, [2] Department of Microbiology

[1,2,3] Periyar University, Salem, Tamil Nadu - 636 011, India.

Abstract: The Schiff base ligand 1-phenyl-3-(pyridin-4-yl) urea was synthesized by condensing substituted pyridines with aryl amines, followed by the preparation of its Pd (II) and Ce (II) complex under reflux conditions. The compounds were characterized using Ultraviolet-Visible spectroscopy (UV-Vis), ^{1}H and ^{13}C-NMR, FT-IR, ESI-MS. The UV-Vis spectrum shows effective formation of the metal complex which is noted due to changes in the charge transfer transitions. Apart from that, there is also L→L and M→L transitions. The NMR studies confirm the formation of the ligand noted by its characteristic regions. The FT-IR spectrum shows efficient formation of the ligands and metal complex. There are changes in the peak region due to coordination of the oxygen atom to the metal compared to ligand. The Mass spectrum shows the molecular ion peak depicting successful formation of the ligand and palladium and cerium metal complex. The anticancer activity of the compounds was assessed using MCF-7 breast cancer cells. The synthesized metal complexes showed good results. They possessed high selectivity with no cytotoxicity for noncancerous cell line. The mode of action and selective toxicity can be understood by further analysis. We assessed the ligand and metal complexes' antibacterial sensitivity, observing variation among microbial species and concentrations. All complexes inhibited growth at 50 µl. Metal complexes (L1-Ce, L3-Pd) showed inhibition zones of 15.0 to 20 mm, whereas ligands (L1-L3) inhibited *Staphylococcus aureus* by 10.0 mm. Out of all the microorganisms examined, *Staphylococcus aureus* showed the highest inhibition at 20.0 mm.

Keywords: Molecular docking, BCL-2, Antibacterial, Anticancer, MCF-7

1.INTRODUCTION

Numerous major studies have been made in analyzing the electronic structure and its co-relation to reactivity in both natural and synthetic systems [1,2]. The chemistry of complexes having rare earth metals is still more to research. Multiply bound rare earth E (E = O, N, P) have a less acidic nature making it more reactive. The rare condition of rare earth E possessing metal -ligand bond is of high polarization. The energy mismatch between both is the cause of the condition [3,4]. Many FDA approved drugs like regorafenib and sorafenib are based on the urea structure. NH–CO scaffold is so reactive to many biomolecules and produces many active pharmacies [5]. Although many attempts have been made towards synthesis of newer drugs, all remain insufficient due to newer antimicrobial resistance and mutant varieties.

Conducting clinical trials has been of great difficulty due to its immense procedures and strict guidelines and synthesis of the newer drugs paves way for newer drug market. All these steps are so long that it makes it so hectic to bring out a novel drug. Coordination chemistry plays a vital role in changing the properties and characteristics of many inorganic compounds [6-13].

Cancer is said to be the second disease in death causing diseases according to WHO. One among six deaths is due to cancer. All the scientists around the world are involved in the synthesis of this cancer curing drug [14]. A vast area of research is dedicated to the cancer biology research. For a drug to be called effective it must pass several criteria. The most important one is the cytotoxicity. The changes in neoplastic cells, receptor over expression, change in membrane fluidity and pH ranges in interstitial area the factors contributing to the greater risk in cancer medicine synthesis. Co-ordination chemistry will offer solutions to problems like longer duration of chemotherapy lasting [15-17]. Palladium is a very precious metal it plays a lot of roles due to its exclusive properties. Palladium is very significant in dental and medical fields. It finds main place in hydrogenation and dehydrogenation reactions. It has very high proficiency in auto catalysis [18-20]. Therefore, vigorous attempts have been made to synthesis complexes out of palladium and cerium. Cc-ordination chemistry plays better roles to combine all the properties of all the beneficial ligands and better properties of metals. So, to synthesis an efficient ligand-metal system for better anticancer activity we have chosen pyridine-based compounds. Herewith we have synthesized homogeneous metal complexes of palladium and cerium and its anticancer activity was analyzed.

2. MATERIALS METHODS

2.1 INSTRUMENTATION

Every chemical employed in this investigation came from a commercial source and was used right away after being refined in accordance with accepted practices. Round-bottom flasks with a capacity of 100 mL were used for conventional reactions. Using a 1:1 mixture of ethyl acetate and n-hexane as the solvent system, Merck pre-coated aluminum sheets of 60 F-254 silica gel plates were subjected to thin-layer chromatography (TLC), which was visible under a UV lamp. The uncorrected melting points were measured using a Buchi melting point BB-545 device with capillary tubes. Using DMSO-d6 as the solvent and TMS as the internal standard, 1H and ^{13}C NMR spectra were captured on a Bruker 400 MHz high-resolution NMR spectrometer. The spectra are presented in parts per million. UV-Vis diffuse reflectance spectra were obtained using an Analytic Jena Specord-200 model, and functional groups were identified using routine FT-IR spectroscopy techniques.

2.2 ANTIBACTERIAL ACTIVITY

With minor adjustments, the agar diffusion method, as outlined by Ranjitha *et al.,* (2023) was used to assess the samples antibacterial activity. Gram-positive *Staphylococcus aureus* MTCC-7443 bacterial strain were used to test the samples. Sterile saline solution was used to modify the inoculum to around 5 × 105 CFU/ml. Samples were placed into various wells with concentrations ranging from 100 µg to 300 µg after being dissolved 10 mg/mL in DMSO as a stock solution. Muller Hinton agar was utilized as the medium, and it was incubated for 24 hours at 37 °C. After the incubation to measure zone of inhibition in (mm).

2.3 CYTOTOXICITY TEST

Cell culture technique: The National Centre for Cell Sciences (NCCS), located in Pune, India, is the source of the human tumor cell line HeLa. The cells were kept in DMEM supplemented with 2 mM l-glutamine and balanced salt solution (BSS) that was adjusted to include 10% fetal bovine serum (GIBCO, USA), 10-mM HEPES (4-(2-hydroxyethyl)-1-piperazine ethane sulfonic acid), 1.5 g/L Na_2CO_3, 0.1 mM nonessential amino acids, 1 mM sodium pyruvate, and 2 mM l-glutamine. The concentrations of streptomycin and penicillin (100 IU/100µg) were adjusted to 1 mL/L. The cells were kept in a humidified CO_2 incubator at 37°C with 5% CO_2.

Evaluation of cytotoxicity: Using an MTT experiment, the inhibitory concentration (^{5}) value was determined. After being seeded in a 96-well plate, cultured cells (1×105) were incubated for 48 hours at 37 °C with 5% CO_2. After 48 hours, the monolayer was rinsed with media, and 100 µL of samples at various test doses were added. The cells were then cultured under the same circumstances for a further 48 hours. After removing the cultured media, 100 µL of the MTT solution was applied to each well, and the wells were incubated for four hours at 37°C. To dissolve the formazan crystals, 100 µL of DMSO was added to each well after the supernatant was removed, and the wells were then incubated for 10 minutes. At 590 nm, the optical density was observed. Using a dose-response curve, the data were represented as IC_{50} values and the percentage growth inhibition was computed.

2.4 MOLECULAR DOCKING STUDY

The three-dimensional structure of ligand was drawn using Chemdraw. The three-dimensional protein structures of BCL-2 were obtained from the PDB database (Reference ID: 6O0K). To obtain the ideal findings during the molecular docking procedure, proteins and ligands are carefully prepared using Auto Dock Tools

1.5.7. PyMOL was utilized to evaluated post-docking outcomes and highlight the important intermolecular interactions that Auto Dock predicted.

3. RESULT AND DISCUSSION

Stoichiometric quantities of unsubstituted arylamine (1) and urea (2) were heated at 90°C in a pilot experiment with 20 weight percent sodium tungstate present. We were pleased to see that the reaction went well and that, in just 30 to 45 minutes, the anticipated 1,3-diphenylurea (3a-c) was produced in 95% yield. The production of metal complexes of cerium and palladium from 1,3-diphenylurea comes next. Using ethanol and sodium tungstate as a catalyst, 1,3-diphenylurea first reacts with metal salts under heating conditions for six hours (Scheme 1). Following this accomplishment, additional surveys were carried out, and Table 1 presents the findings. Under the same circumstances, but without sulfated tungstate, an experiment was conducted to evaluate the catalytic function of sodium tungstate. The fact that this reaction only produced 0% after 24 hours (Table 1, entry 1) shows how important sulfated tungstate is as a catalyst for increasing reaction pace and efficiency. By conducting the reaction with 5 weight percent, 10 weight percent, and 15 weight percent of the catalyst, the catalyst loading was tuned. The findings demonstrated that a 15-weight percent catalyst loading was ideal, with 45% yield after 4 hours at 5 weight percent (Table 1, entry 2), 60% yield after 4 hours at 10 weight percent (Table 1, entry 3), and 94% yield in under 40 minutes at 15 weight percent (Table 1, entry 4). Since reactions at 70°C, 60°C, and room temperature gradually produced less amounts of the product 60% at 70°C in 4 hours, 55% at 60°C in 5 hours, and 0% at room temperature it was determined that 90°C was the optimal reaction temperature (Table 1, entries 5-7). Additionally, reactions were conducted in polar and non-polar solvents, including hexane, ethanol, methanol, and water. In non-polar circumstances, no product was generated (Table 1, entry 8); in other solvents, the results were disappointing, with water and methanol exhibiting negligible product formation (Table 1, entries 9-10). Lastly, all reactions were carried out at 90°C with a catalyst loading of 15 weight percent in ethanol as the solvent to investigate the substrate scope.

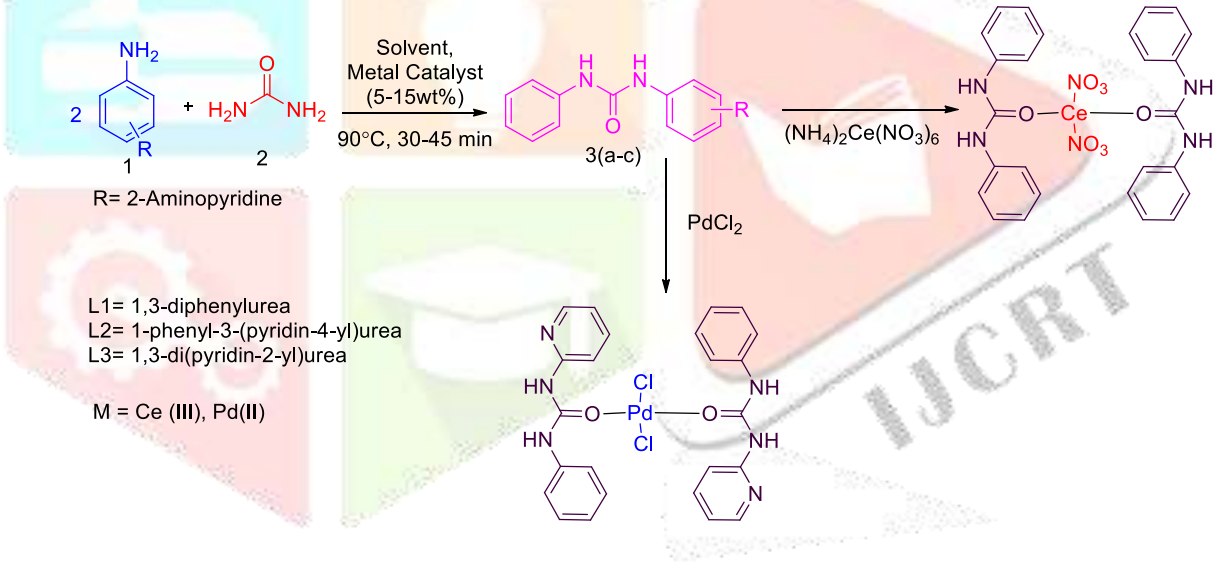

Scheme 1: Synthesis of Ligand and Metal complexes

Table 1: Catalytic performance of the synthesized ligands

Entry	Catalytic %	Temperature (°C)	Solvent	Yield (%)
1	-	90	Ethanol	NR
2	5 w%	90	Ethanol	45
3	10w%	90	Ethanol	60
4	**15w%**	**90**	**Ethanol**	**94**
5	15w%	70	Ethanol	60
6	15w%	60	Ethanol	55
7	15w%	RT	Ethanol	NR
8	15w%	90	Hexane	NR
9	15w%	90	Methanol	92
10	15w%	90	Water	80

3.1 FT-IR SPECTRA

The functional groups and chemical structures in **Fig.** 1 can be verified by the observed peaks alone. The 1,2,4-trisubstituted band, N–O stretching, and CH_2 bending are responsible for the Ce complex's peaks at 1497, 1288, and 828 $^{cm-1}$, respectively. Around 3600 $^{cm-1}$, NH stretching vibrations are detected. Stretching vibrations for C=O were detected at about 1600 $^{cm-1}$. Around 1400–1300, the C–H deformation band revealed ligand formation. The M-N bond is observed usually from the frequency around 330 $^{cm-1}$. The wavenumber region is around 400 due to Pd-Cl in PdL2. All the peaks show blue shifts after coordination with the metal ion.

3.2 UV VISIBLE SPECTRA

In ligand $\pi \rightarrow \pi^*$ and n$\rightarrow \pi^*$ transitions were found around 200-400 nm region in **Fig.** 2. But in metal complexes additional bands above 400 nm were witnessed due to LMCT transitions. Palladium (II) complexes exhibit diamagnetic properties. The spectra of palladium (II) complexes possess bands at 300 nm due to Pd-charge-transfer transitions. Studies using UV-visible absorption spectroscopy revealed that CeL1, PdL2, PdL3, and CeL2 had an LMCT band at 454, 448, 532, and 436 (**Fig.** 2). Three bands at 280 nm, 298 nm, and 291 nm were produced via Gaussian fits to the absorption band data. Considering the proligand's 228 nm absorption peak, the 280 nm band was designated as a ligand-based transition.

3.3. MASS SPECTRA

The electron impact mass spectra of ligands L1-L3 and their metal complexes were recorded and analyzed at an energy of 70 eV. The mass spectra and proposed fragmentation pathways for L1 are presented in **Fig.** 3-4. The molecular ion peaks were found to align with the expected values based on the elemental analysis, confirming the molecular formulas. The exact masses of the ligands are L1 - 212.0950, L2 - 213.0902, and L3 - 214.0855. These values correspond to the theoretical mass values for the formulas $C_{13}H_{14}N_2$, $C_{12}H_{11}N_3O$, and $C_{11}H_{10}N_4O$, respectively, as determined through the mass spectral fragmentation technique. Additionally, the mass spectra of the metal complexes L1Ce, L2Ce, L2Pd, and L3Pd are shown in **Fig.** 3. The complexes correspond to the following formulas: L1Ce - $C_{26}H_{24}CeN_6O_8$, L2Ce - $C_{24}H_{22}CeN_8O_8$, L2Pd - $C_{24}H_{22}Cl_2N_6O_2$ Pd, and L3Pd - $C_{22}H_{20}Cl_2N_8O_2$ Pd. The exact masses of these complexes are 688.07, 690.06, 602.02, and 604.01 m/z, respectively. In all cases, the fragmentation patterns of both the ligands and their corresponding metal complexes were consistent with the expected molecular weights, confirming the structures proposed. The results from the ESI mass spectra are summarized in Table 2. Mass values of Ligand and Metal complexes.

Table 2: Mass value of ligand and metal complexes

Compound	Calculated	Found
L1	212.095 m/z	212.095 m/z
L2	213.0902 m/z	213.0902 m/z
L3	214.0855 m/z	214.0855 m/z
L1Ce	688.07 m/z	688.07 m/z
L2Ce	690.06 m/z	690.06 m/z
L2Pd	602.02 m/z	602.02 m/z
L3Pd	604.01 m/z	604.01 m/z

3.4 NMR

The ligand and its complex (L1-L1-Ce) exhibit signals in the anticipated regions of their ^{1}H NMR spectra. The enolization and coordination of the thiolate sulfur to the Ce (II) ion were supported by the singlets that appeared for the C–NH–C=O proton of the free ligand at 8.53 ppm in the ligand spectra. These singlets vanished upon complexation, which verified amine imine tautomerism, followed by deprotonation upon coordination with metal. The –NH protons have been identified as the source of the singlet at 8.68–8.63 ppm found in the complicated spectra. Additionally, the ligand aromatic hydrogen spectra were found in the 7.305–5.654 ppm range, whereas the complex's aromatic protons were found in the 8.01–5.53 ppm range. The ligand and its complex (L2-L2-Ce and L2-Pd) exhibit signals in the anticipated regions of their ^{1}H NMR spectra. The enolization and coordination of the thiolate sulfur to the Ce (II) ion and Pd (II) ion were supported by the disappearance of the singlets that appeared for the C–NH–C=O proton of the free ligand at 8.34-8.25 ppm in the ligand spectra upon complexation, which confirmed amine imine tautomerism followed by deprotonation

upon coordination with metal. For the Ce and Pd complex, respectively, the spectra revealed a singlet at 8.562–8.558 ppm and 8.824–8.279 ppm, which has been attributed to -NH protons. Additionally, the ligand's aromatic hydrogen spectra were found in the 6.58–5.21 ppm range, while the complexes' aromatic protons were found in the 7.838–5.571 ppm range for the Ce (II) complex and the 7.681–5.554 ppm range for the Pd (II) complex.

The ligand and its complex (L3-L3-Pd) exhibit signals in the anticipated regions of their ^{1}H NMR spectra. The enolization and coordination of the thiolate sulfur to the Pd (II) ion were supported by the disappearance of the singlets that appeared for the C–NH–C=O proton of the free ligand at 8.34–8.33 ppm in the ligand spectra upon complexation, which confirmed amine imine tautomerism followed by deprotonation upon coordination with metal. The complex spectrum revealed a singlet at 8.310–5.562 ppm that has been attributed to –NH protons. Additionally, the ligand's aromatic hydrogen spectra were found in the 8.02–5.44 ppm range, whereas the complex's aromatic protons were found in the 8.31–5.56 ppm range (**Fig.** 5).

The formation of amide (I) occurs initially through a condensation reaction between an arylamine and urea, with the elimination of ammonia. Next, the addition of another equivalent of arylamine leads to a nucleophilic substitution on the carbonyl group, forming compound II. Finally, deprotonation of compound II yields the corresponding product, 1,3-diphenylurea (compound III).

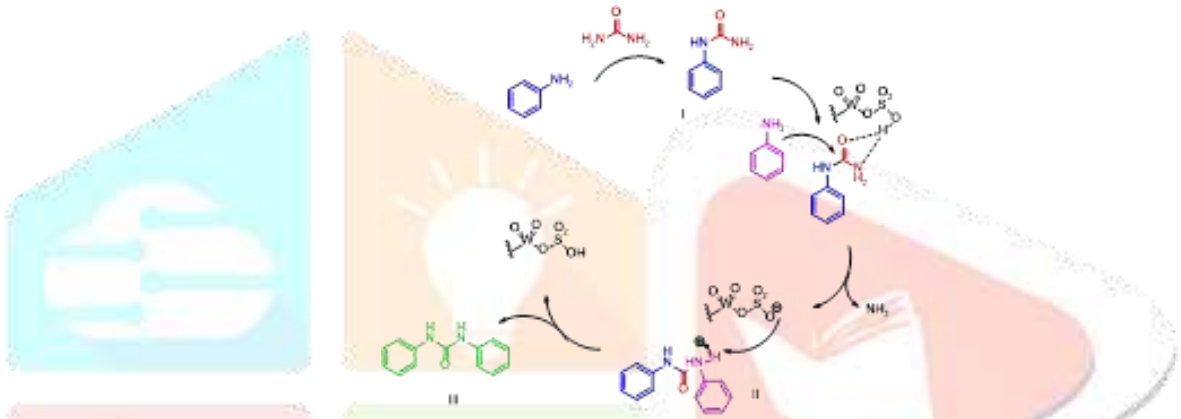

Scheme 2: Proposed mechanism of synthesized ligands

3.5 ANTIBACTERIAL ACTIVITY

We have evaluated the ligand and metal complexes antibacterial sensitivity and found that it varies according to the microbial species and the ligand and metal complex concentrations. Zones of inhibition were created at the single concentration of 50 µl that we established. The antibacterial activity of ligand and metal complexes was evaluated using the well diffusion method and a range of pathogens, including gram-positive bacteria *Staphylococcus aureus* (**Fig.** 6). The results indicate that ligand (L1-L3) exhibited antibacterial activity against *Staphylococcus aureus* with a recorded zone of inhibition of 10.0 mm at a concentration of 50 µl. For metal complexes (L1-Ce, L3-Pd metal complexes), the zone of inhibition was 15.0-20 mm against *Staphylococcus aureus*. The compounds demonstrated good activity against *Staphylococcus* species, although *Staphylococcus aureus* showed a zone of inhibition of 20.0 mm. Among all microorganisms tested, *Staphylococcus aureus* exhibited the most significant zone of inhibition (Table 3).

Table 3: Antibacterial activity zone of inhibition of ligand and metal complexes

S. No	**Name of sample(µg)** (Ligand & Meatal complexes)	**Zone of inhibition (mm)**
		Staphylococcus aureus
1	L1	10
2	L2	5
3	L3	4
4	L1-Ce	15
5	L3-Pd	20
6	Tetracycline (Control)	24

3.6 ANTICANCER ACTIVITY

In this study, we investigated cell viability in MCF-7 cells treated with various concentrations of synthesized Pd metal complex (L3Pd), alongside positive controls (anastrozole), using the MTT assay. MCF-7 cells were exposed to concentrations ranging from 25 and 50 µg/ml for Pd metal complex and the controls. We monitored cell viability over a 24-hour period, with results shown in **Fig.** 7. As the doses of Pd metal complex, anastrozole, and celecoxib increased, we observed a decrease in cell viability and an increase in cytotoxicity. Both Pd metal complex and anastrozole demonstrated dose-dependent cytotoxic effects in MCF-7 cells, with IC_{50} values of 42.51 µg/ml for Pd metal complex and 24.7 µg/ml for anastrozole, indicating that Pd metal complex exhibit greater cytotoxic activity compared to anastrozole.

3.7 MOLECULAR DOCKING STUDIES

The molecular docking study of the synthesized ligand (Lig) with the anti-apoptotic BCL-2 protein was performed to understand its binding mechanism and its possible role in inducing apoptosis in MCF-7 breast cancer cells. The docking score of the Lig-BCL2 complex was -6.56 kcal/mol, indicating a strong and stable binding affinity toward the BCL-2 active site and Table 4. represents Docking score of BCL2 with Pd metal complex (L3Pd). As shown in **Fig. 8**(a–c), the ligand is well-fitted into the hydrophobic cavity of BCL-2 and stabilized by multiple hydrogen bonds and hydrophobic interactions. The hydrogen bonding residues include Ala100 (2.7 Å), Asp103 (2.2 Å), Phe104 (2.1 Å), Tyr108 (2.6 Å), Trp144 (2.4 Å), Gly145 (2.0 Å), and Tyr202 (2.1 Å), while hydrophobic interactions were observed with Ala100 (4.8 Å), Arg146 (4.1 Å), Ala149 (4.4 Å), and Tyr202 (3.6 Å). These interactions are crucial for the ligand's firm anchoring within the BCL-2 binding pocket. The 3D visualization (**Fig**. 8a) clearly demonstrates key hydrogen bonds that enhance stability, while (**Fig.** 8b) displays the ligand orientation within the BCL-2 secondary structure. The surface representation in (**Fig.** 8c) highlights how the ligand is deeply embedded within the hydrophobic pocket of BCL-2, ensuring strong molecular contact. Since BCL-2 is known to prevent apoptosis by inhibiting mitochondrial cell death pathways, the effective binding of the ligand may inhibit BCL-2s anti-apoptotic function. Consequently, this interaction could promote apoptosis in MCF-7 breast cancer cells, thereby explaining the observed anticancer activity in vitro. Finally, the docking results support the experimental anticancer findings, suggesting that the ligand may induce cell death in MCF-7 cells through BCL-2 inhibition, disrupting cancer cell survival mechanisms and enhancing apoptotic signaling. Table 5. represents Intermolecular interactions of BCL2 with Pd metal complex. (L3Pd)

Table 4: Docking score of BCL2 with Pd metal complex (L3Pd)

Complex	Dock Score (kcal/mol)	Grid dimension
Lig-BCL2	-6.56	40×46×52-12.804×5.45×-7.481

Table 5: Intermolecular interactions of BCL2 with Pd metal complex. (L3Pd)

Complex	Hydrogen bonding interactions (Distance in Å)	Hydrophobic interactions (Distance in Å)
Lig-BCL2	Ala100 (2.7), Asp103 (2.2), Phe104 (2.1), Tyr108 (2.6), Trp144 (2.4), Gly145 (2.0), Tyr202 (2.1)	Ala100 (4.8), Arg146 (4.1), Ala149 (4.4), Tyr202 (3.6)

3.8 ADME STUDIES

The Boiled-Egg plot shown illustrates the relationship between the molecule's polarity (TPSA) and lipophilicity (WLOGP), which are key indicators of its pharmacokinetic behavior. In this model, the yellow and white oval regions represent the zones of molecules that can penetrate the blood–brain barrier (BBB) and those that have good gastrointestinal (GI) absorption, respectively. The red-marked Molecule 1 lies outside both the yellow and white regions, with a TPSA value around 100 Å² and a WLOGP value near 6.0. This

suggests that the compound has high lipophilicity and moderate polarity, which may limit its oral absorption and brain permeability. However, the high lipophilic nature of the molecule can enhance its interaction with lipid-rich cellular membranes, improving uptake into cancer cells such as MCF-7 breast cancer cells. Therefore, while the compound may not be ideal for oral or CNS applications, its physicochemical characteristics support its potential as an effective intracellular anticancer agent through enhanced cell membrane penetration and binding with key targets like the BCL-2 protein (**Fig.** 9). and Table 6. List out the In Silico ADMET and Toxicity Profile of Ligand (LIG)

Table 6: In Silico ADMET and Toxicity Profile of Ligand (LIG)

Category	Parameter	Value / Result	Interpretation / Comment
Physicochemical	Molecular Weight	603.80	Slightly above optimal range (100–600); may reduce permeability.
	TPSA	108.04	Within optimal range (0–140); indicates acceptable permeability.
	LogP	0.00	Poor lipophilicity.
	LogS	-8.82	Poor solubility.
Medicinal Chemistry	QED (Drug-likeness)	0.282	Moderate; acceptable but not highly drug-like.
	Lipinski Rule Compliance	1 violation	Good oral bioavailability potential.
	Golden Triangle Compliance	0.0	Favorable ADMET profile.
	PAINS Alerts	None	No reactive or promiscuous behavior.
Absorption	P-gp Inhibition	Strong inhibitor	May cause drug–drug interactions.
	Human Intestinal Absorption	Poor	Low intestinal permeability.
	Bioavailability	55%	Moderate; suitable for oral administration.
Distribution	BBB Penetration	0.85	Moderate CNS penetration; potential CNS-active compound.
Metabolism	CYP1A2	0.67 (Strong inhibitor)	May cause metabolic interactions.
	CYP2C19	0.80 (Strong inhibitor)	Significant inhibition potential.
	CYP2C9	0.56 (Not inhibitor)	Minimal effect.
	CYP2D6	0.75 (Not inhibitor)	Moderate; not a major concern.
	CYP3A4	0.78 (Strong inhibitor)	Potential for drug–drug interactions.
Toxicity	Mutagenicity	0.54 (Poor)	Low genotoxic risk.
	Respiratory Toxicity	0.54 (Moderate)	Moderate toxicity risk.
	Carcinogenicity	0.59 (Moderate)	Moderate carcinogenic potential.
	Hepatotoxicity	0.50 (Poor)	Possible liver toxicity.
	Nephrotoxicity	0.59 (Good)	May induce kidney toxicity.
	Neurotoxicity	0.74 (Moderate)	Moderate neurotoxic risk.
	Cardiotoxicity	0.86 (Good)	Favorable cardiac safety.
	Immunotoxicity	0.95 (Moderate)	Moderate immune toxicity.
	Nutritional Toxicity	0.51 (Poor)	Low nutritional safety.
	Cytotoxicity	0.60 (Moderate)	Acceptable cellular toxicity.

Environmental	Eco-toxicity	0.52 (Good)	Acceptable environmental safety.

4. CONCLUSION

We have synthesized four metal complexes: L1Ce, L2Ce, L2Pd, and L3Pd using different ligands. The structures of these metal complexes and ligands were confirmed through ^{1}H-NMR, ^{13}C-NMR, FT-IR, UV-Vis, and mass spectroscopic techniques. Based on these studies, the correct structures were identified, with the –NH protons and aromatic protons observed at chemical shifts of 8.68–8.63 ppm and 7.305–5.654 ppm, respectively, in the NMR spectra. The exact mass values were consistent across all metal complexes and ligands. The UV-Vis spectra showed absorption maxima above 454 nm and 448 nm, which indicated the formation of the metal complexes. Furthermore, selected metal complexes were evaluated for their anticancer activity against MCF-7 cells, demonstrating a promising IC_{50} value of 42.51 µg/ml.

ACKNOWLEDGEMENT

We would like to express our sincere thanks to Periyar University for provide University Research Fellowship (URF) their support and contribution to this research.

AUTHOR CONTRIBUTIONS

Periyannan Muniyappan: Conceptualization, Methodology, Software, Validation, Investigation, Resources and Writing Original Draft; **Santhakumar Munusamy:** Biological activities and validation of results and manuscript editing; **Rajavel Rangappan:** Software, validation, Review & Investigation.

FUNDING

Not applicable

CONFLICT OF INTEREST

No conflict of interest

DATA AVAILABILITY STATEMENT

All data available in the manuscript

REFERENCES

[1]. Solola, L. A., Zabula, A. V., Dorfner, W. L., Manor, B. C., Carroll, P. J., & Schelter, E. J. (2017). Cerium (IV) imido complexes: structural, computational, and reactivity studies. *Journal of the American Chemical Society*, 139(6), 2435-2442.

[2]. Nugent, W. A., & Mayer, J. M. (1988). Metal-ligand multiple bonds: the chemistry of transition metal complexes containing oxo, nitrido, imido, alkylidene, or alkylidyne ligands.

[3]. Raymond, K. N., & Eigenbrot Jr, C. W. (1980). Structural criteria for the mode of bonding of organoactinides and-lanthanides and related compounds. *Accounts of Chemical Research*, 13(8), 276-283.

[4]. Summerscales, O. T., & Gordon, J. C. (2013). Complexes containing multiple bonding interactions between lanthanoid elements and main-group fragments. *RSC advances*, 3(19), 6682-6692.

[5]. Anam, R. P., Saeed, U., Ajmal, K., Ahsan, S., Javid, H., Tanzila, R., Rimsha, T., Rima, D. A., Hamdy, K., Magda, H. A., Ahmed, A., & Zahid, S. (2024). Synthesis and biological evaluation of metal complexes with antimicrobial potential. *RSC Advances, 14*, 29288–29297.

[6]. Petkov, N., Pantcheva, I., Ivanova, A., Stoyanova, R., Kukeva, R., Alexandrova, R., Abudalleh, A., & Dorkov, P. S. T. (2020). Medicinal applications of coordination complexes. *Journal of Physics: Conference Series*, 1664, 012070.

[7]. Gasser, G. (2015). Metal-based drugs: new opportunities in medicinal chemistry. Chimia, 69, 442–446.

[8]. Habala, L., & Valentová, J. (2020). Recent advances in metal-based pharmaceuticals. *Česká a slovenská farmacie*, 69, 121–129.

[9]. Bao, G. (2020). Luminescent cerium complexes for biomedical applications. Journal of Luminescence, 228, 117622.

[10]. Kontoghiorghes, G. J. (2020). Chelation therapy and molecular targeting in medicine. *International Journal of Molecular Sciences*, 21, 2499.

[11]. Siegel, R. L., Miller, K. D., & Jemal, A. (2018). Cancer statistics, 2018. *CA: A Cancer Journal for Clinicians, 68*, 7–30.

[12]. Petkov, N., Pantcheva, I., Ivanova, A., Stoyanova, R., Kukeva, R., Alexandrova, R., Abudalleh, A., & Dorkov, P. S. (2023). Synthesis, structure, and biological evaluation of transition metal complexes. *Molecules, 28*, 4676.

[13]. Akl, M. A., El Mahdy, N. A., & El Gharkawy, E. S. R. H. (2022). Novel metal complexes with enhanced cytotoxic properties. *Scientific Reports, 12*, 17451.

[14]. Zhenjun, M., Haorui, G., & Xufeng, L. (2021). Catalytic and biological activity of cerium-based complexes. *Catalysts*, *11*(9), 1078.

[15]. Bin, X., Yufeng, C., Yujuan, Z., Bangsheng, Z., Guiqing, L., Qian, L., Yongbin, Y., & Tao, J. (2022). Structural and functional analysis of metal complexes. *Metals*, *12*(4), 533.

[16]. Oliveira, C. G., Maia, P. I. da S., Souza, P. C., Pavan, F. R., Leite, C. Q. F., Viana, R. B., Batista, A. A., Nascimento, O. R., & Deflon, V. M. (2014). Synthesis and evaluation of ruthenium (II) complexes as potential antitubercular agents. *Journal of Inorganic Biochemistry*, *132*, 21–30.

[17]. Lopes, E. O., Oliveira, C. G., Silva, P. B., Eismann, C. E., Suárez, A. C., Menegário, A. A., Leite, C. Q. F., Deflon, V. M., & Pavan, F. R. (2016). Biological activity of new organometallic complexes. *International Journal of Molecular Sciences, 17*, 1–10.

[18]. Jiang, Z. G., Lebowitz, M. S., & Ghanbari, H. A. (2006). Neuroprotective effects of metal-based compounds. *CNS Drug Reviews, 12*, 77–88.

[19]. Li, T. K., & Liu, L. F. (2001). Mechanisms of action of metal–DNA binding agents. *Annual Review of Pharmacology and Toxicology, 41*, 53–77.

[20]. Yalowich, J. C., Wu, X., Zhang, R., Kanagasabai, R., Hornbaker, M., & Hasinoff, B. B. (2012). DNA damage and apoptotic mechanisms induced by coordination complexes. *Biochemical Pharmacology, 84*, 52–63.

Figures

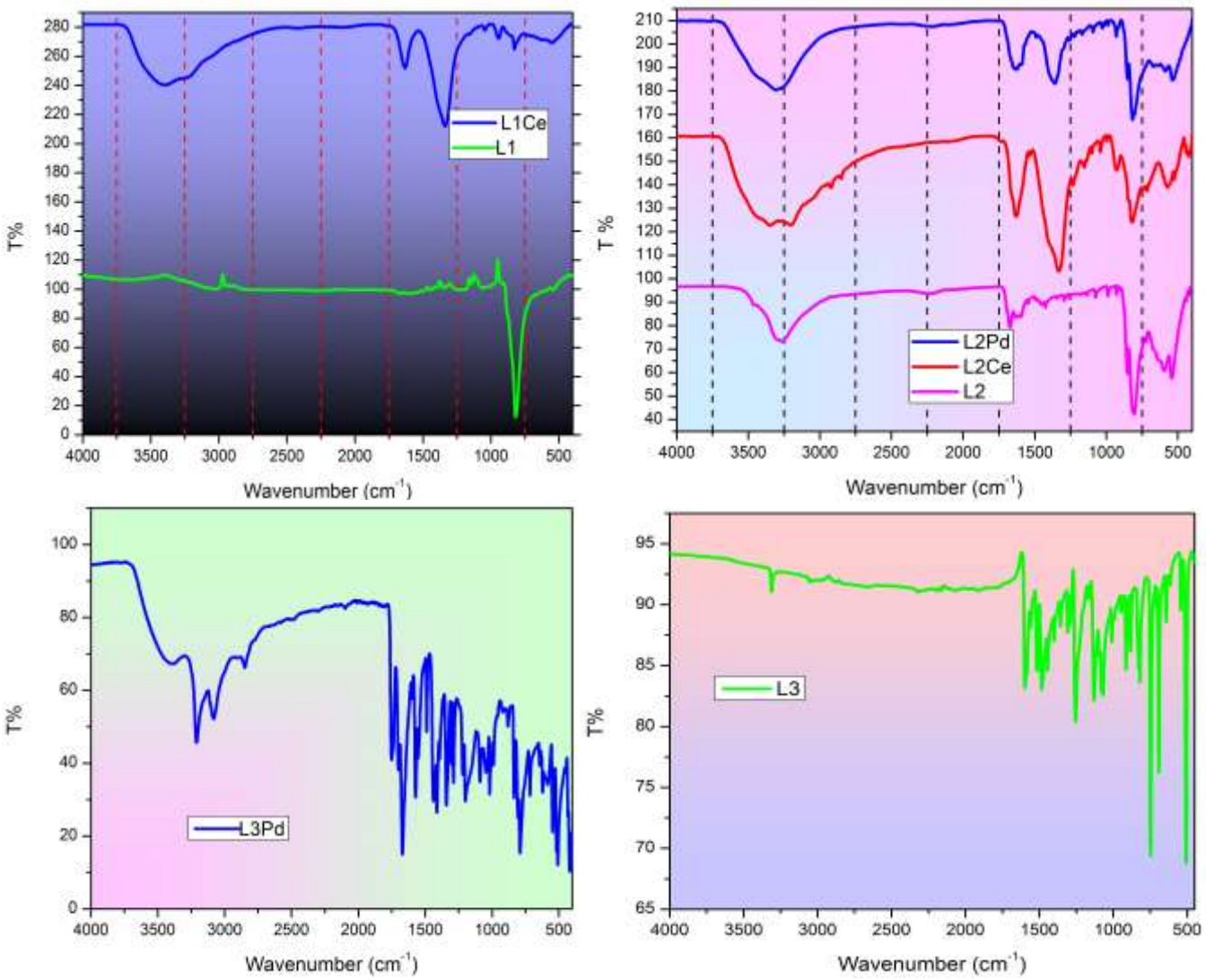

Figure 1. FT-IR Spectrum of synthesized Ligands and Metal complexes

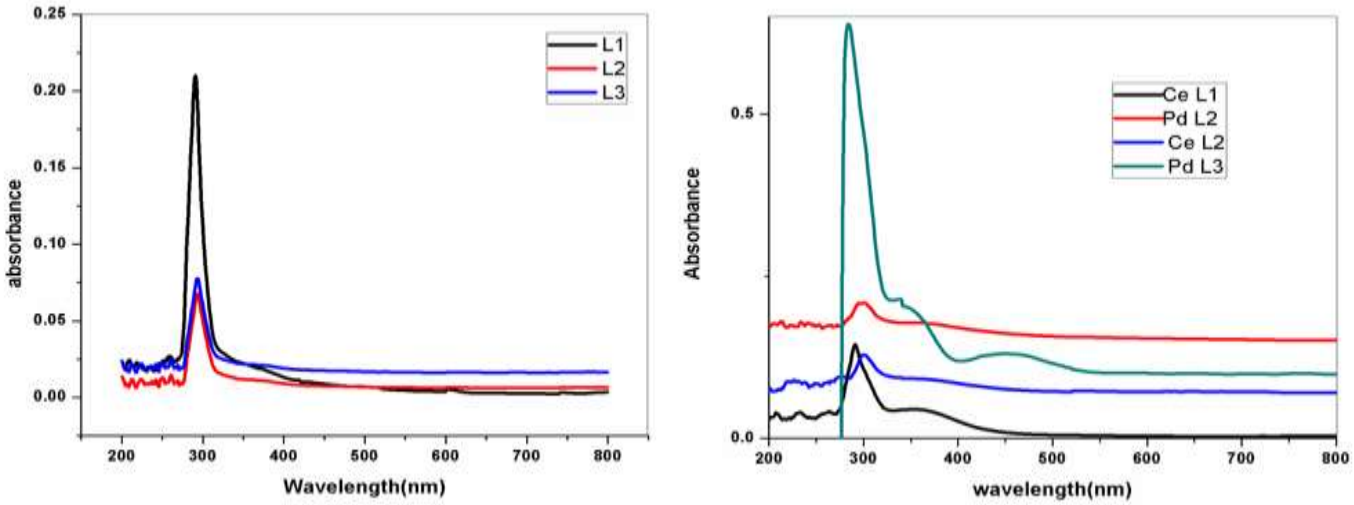

Figure 2. UV-Vis Spectrum of synthesized Ligands and Metal complexes

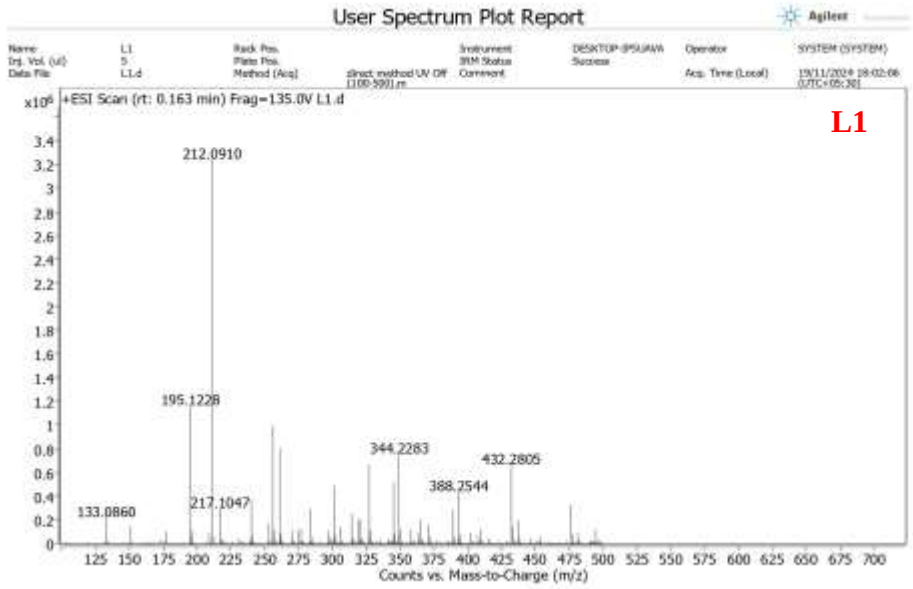

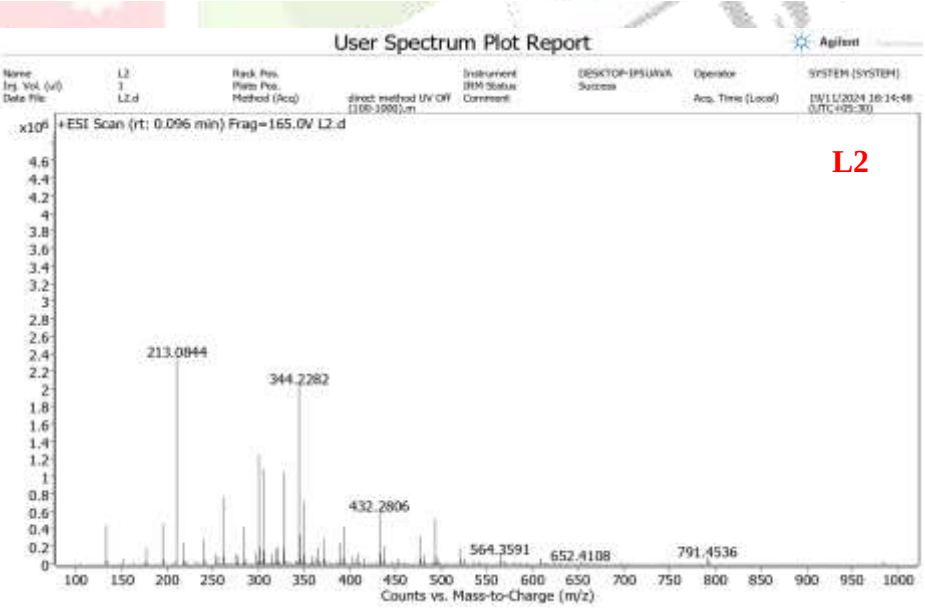

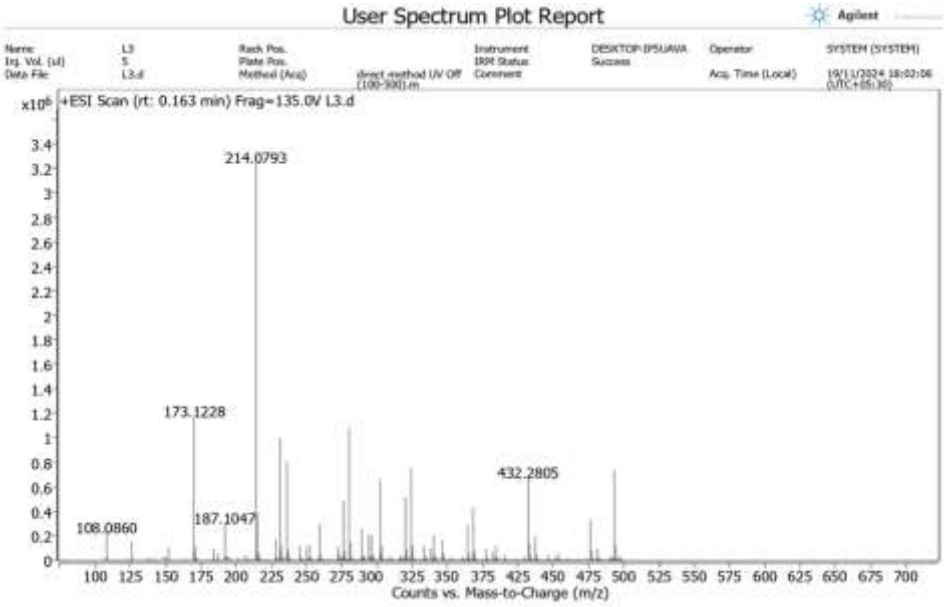

L3

Figure 3. Mass Spectrum of synthesized Ligands

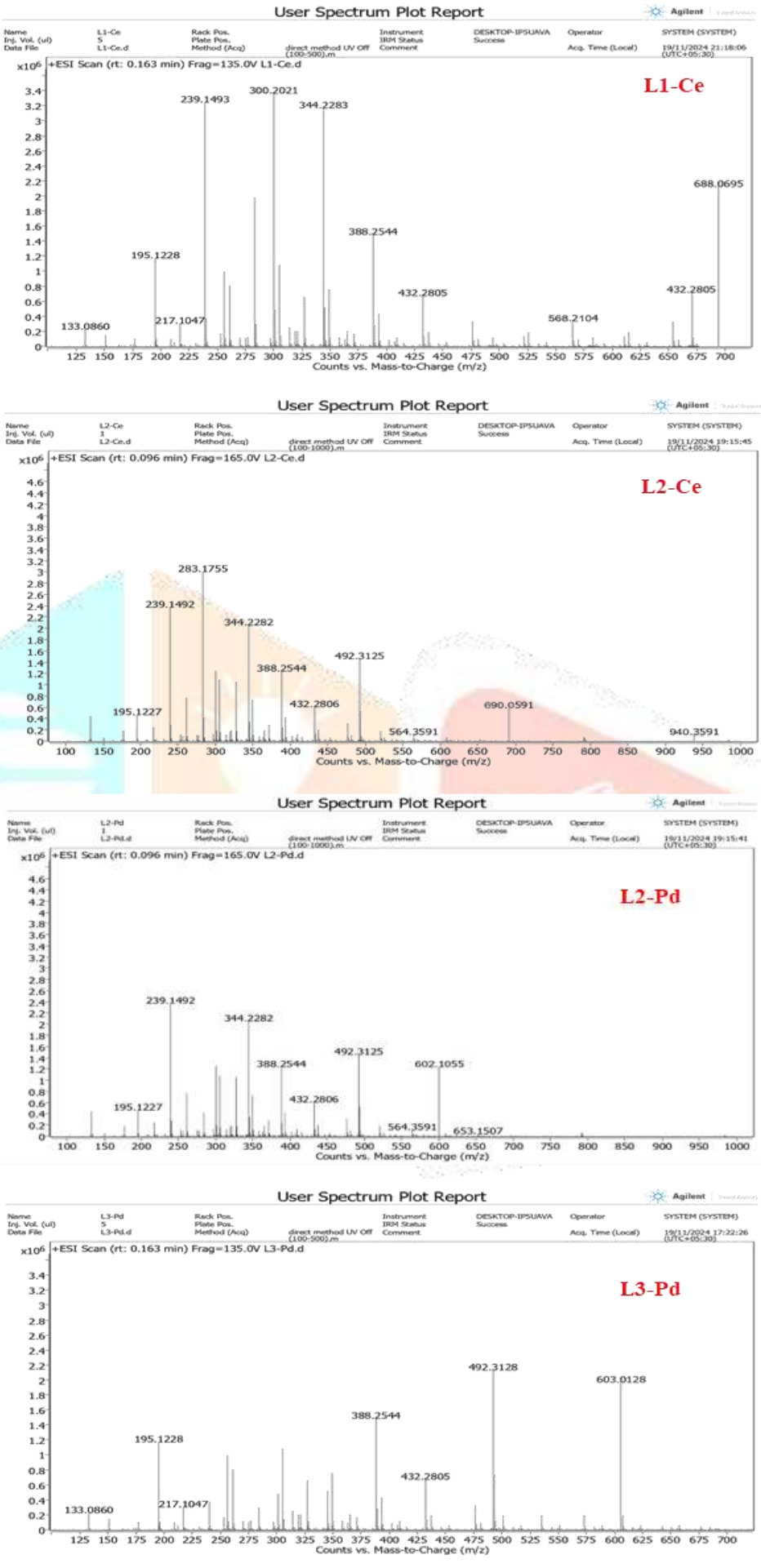

Figure 4. Mass Spectrum of synthesized Metal complexes

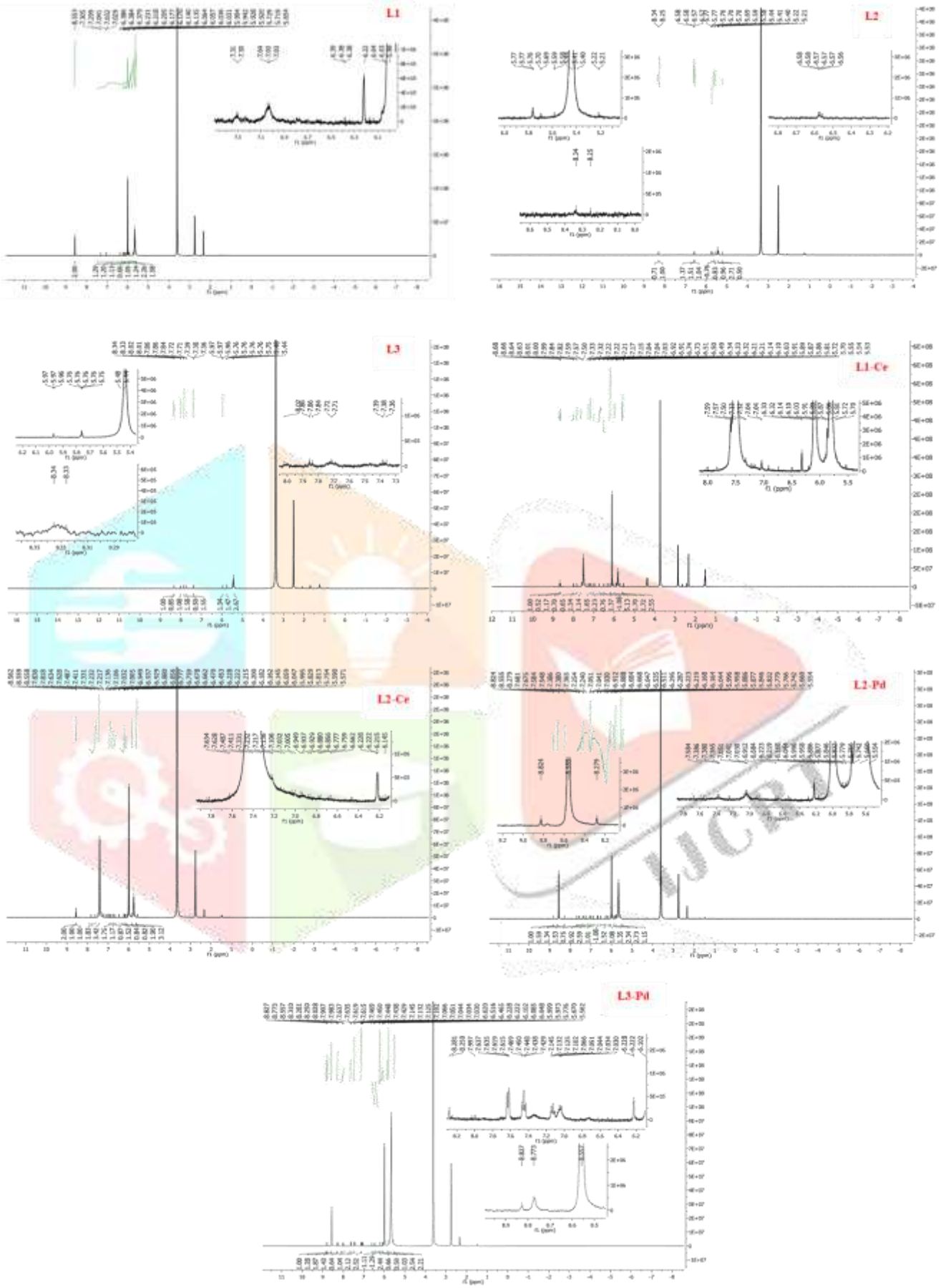

Figure 5. NMR Spectrum of synthesized Ligands and Metal complexes

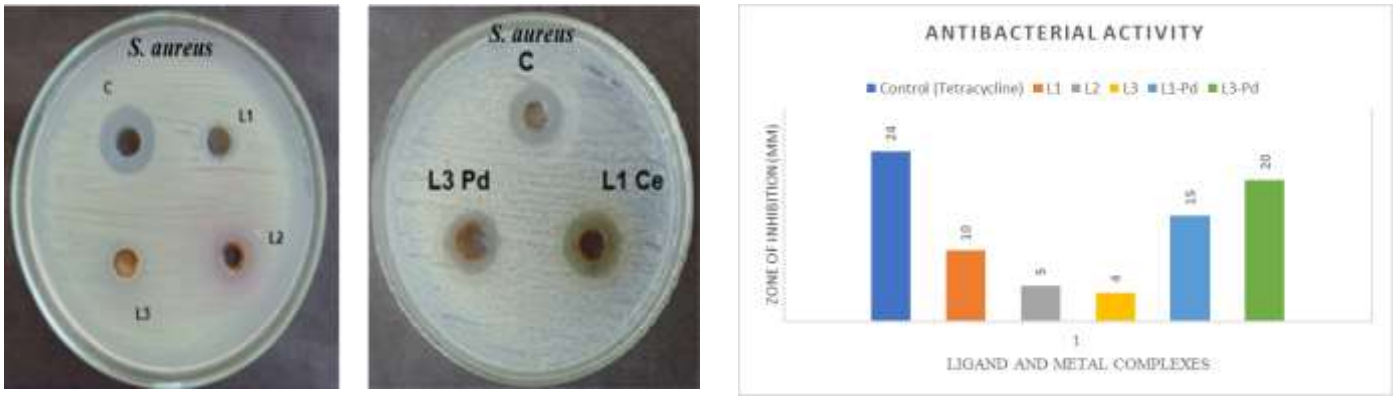

Figure 6. Antibacterial activity of ligand and metal complexes

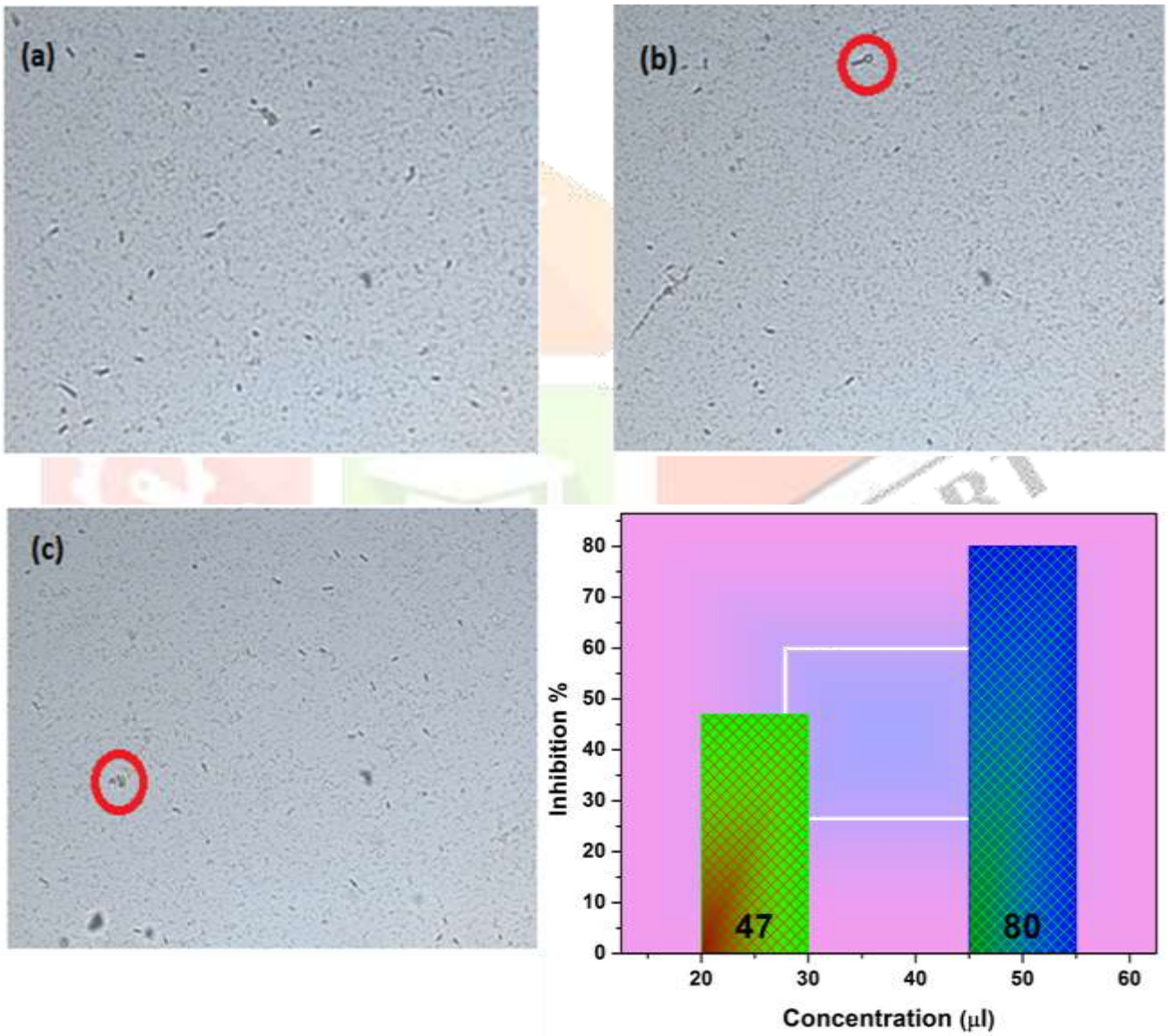

Figure 7: Cell viability after treatment of MCF-7cells with different concentrations of synthesized nanoparticles (25, and 50 µg/ml). The result was expressed as percentage cell viability. (a) control (b) 25 µg/ml, (c) 50 µg/ml, of Pd metal complex.

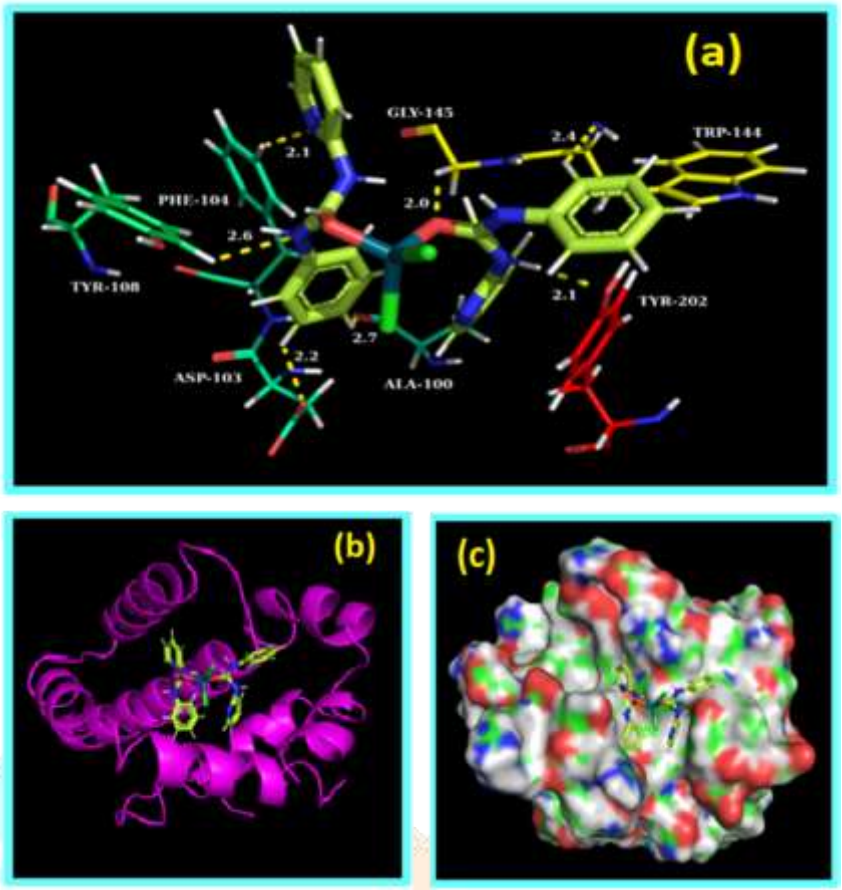

Figure 8: Molecular docking studies (a) Pd metalcomplex.is placed at the mouth of the active site where it forms hydrogen bonds with key residues stabilizing its interaction with BCL2. (b) The cartoon representation illustrates the secondary structure elements stabilizing the BCL2 with Pd metal complex., (c) The surface view of BCL2 reveals distinct binding cavities where Pd metal complex. interacts with key residues.

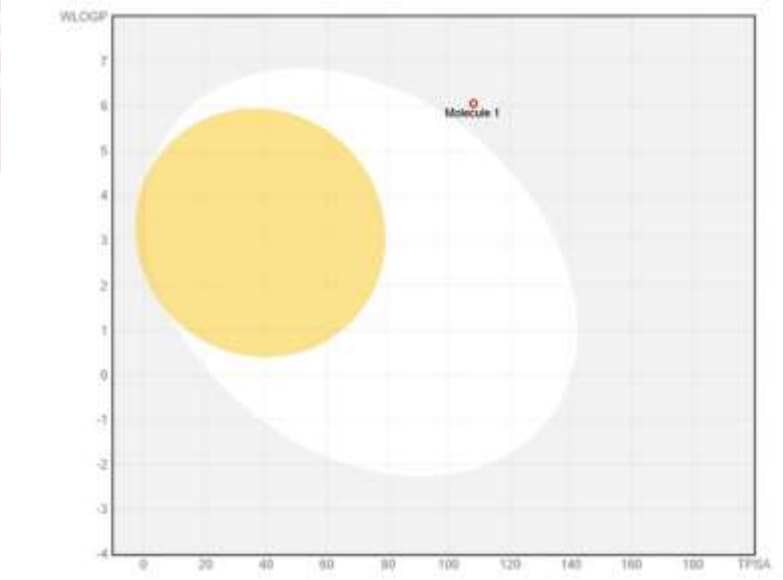

Figure 9: Boiled-Egg view of Pd metal complex(L3Pd)